Partially Stirred Reactor: Study of the Sensitivity of the Monte-Carlo Simulation to the Number of Stochastic Particles with the use of a Semi-Analytic, Steady-State, Solution to the PDF Equation

VLADIMIR A. SABEL'NIKOV*

Department Energétique Fondamentale et Appliquée, Office National d'Etudes et de Recherches Aérospatiales, Fort de Palaiseau 91761, Palaiseau Cedex France

and

LUIS FERNANDO FIGUEIRA DA SILVA†

Laboratoire de Combustion et de Détonique, Centre National de la Recherche Scientifique, 86961 Futuroscope Chasseneuil, France

The development of low pollutant emission hydrocarbon fuel engines requires well adapted turbulent combustion models. Partially Stirred Reactor (PaSR) models have been developed to deal with pollutant formation. These models are essentially based on the application of a stochastic Monte-Carlo process to determine the solution of the transport equation for the joint probability density function (pdf) for all reactive species. In this work the semi-analytic, steady-state, solution of the transport equation of the pdf of a single reacting scalar, whose chemistry is described by an Arrhenius law and by employing the Interaction by Exchange with the Mean micro-mixing model, within a PaSR is presented. The overall characteristics of this solution are discussed, with emphasis on the role played by the ratios between the residence time and the micro-mixing and chemical times, respectively. Then, a comparison is made between this solution and a numerical solution of the PaSR model equations using a Monte-Carlo technique. This comparison evidences the number of particles required for an accurate numerical computation, which is a function of the aforementioned ratios.

INTRODUCTION

The development of low pollutant emission hydrocarbon fuel engines requires well adapted turbulent combustion models. Most models currently used for the prediction of the combustion process, for instance, flamelet [1–4] and conditional moment closure models [5] are based on the hypothesis that the characteristic time of the chemical reactions is small when compared to the Kolmogorov time scale, which characterizes the smallest eddy-turnover time. This hypothesis is most often satisfied in practical systems as far as the chemical heat release is concerned. On the contrary, the formation of pollutant species, such as CO and NO_x, may occur in time scales that are much longer than the heat release time.

Partially Stirred Reactor (PaSR) models have been developed to account for finite micro-mixing times, that is, the presence of scalar fluctuations, and thus to deal with pollutant formation [6–8]. These models are essentially based on the application of a stochastic Monte-Carlo process [9] to determine the joint probability density function (pdf) for all reactive species. It was shown that PaSR models with Monte-Carlo simulation technique, which computes the chemical production exactly and requires modeling of the micro-mixing process, that is, the mixing at the molecular scale, has the potential to essentially improve the predictions of pollutant emissions. However, Monte-Carlo simulations require the presence of stochastic particles in sufficient number throughout the flowfield, so that the statistics of the computed quantities (species mass fractions, etc.) can be correctly predicted. For complex systems involving multiple chemical reactions, the knowledge of the number of particles required can only be gathered by performing a study of the sensitivity

*Corresponding author: E-mail: Vladimir.Sabelnikov@onera.fr

†L. F. Figueira is currently at Departmento de Engenharia Mecânica; Pontifícia Universidade Católica do Rio de Janeiro; 22453–900, Rio de Janeiro - RJ - Brazil.

0010-2180/02/$–see front matter
PII 0010-2180(02)00336-X

COMBUSTION AND FLAME 129:164–178 (2002)

Published by Elsevier Science Inc.

of the solution to the number of stochastic particles present [10]. Moreover, the problem of assessing the quality of the computed solution is worsened by the fact that the statistical distribution of each species mass fraction is unknown a priori. The study of simplified systems, such as the PaSR, may provide relevant information concerning both the overall shape of the pdf of reactive scalar and the sensitivity of the computed solution to the number of stochastic particles.

In this work the semi-analytic, steady-state, solution of the transport equation of the pdf of a single reacting scalar, for the case of non-trivial chemical reaction rate (Arrhenius law) and by employing the Interaction by Exchange with the Mean (IEM) micro-mixing model, within a PaSR is presented. The solution is obtained after a series of analytical transformations and analysis, followed by a numerical solution in the final step. The overall characteristics of this solution are discussed, with emphasis on the role played by the dimensionless ratios between the residence time and the micro-mixing and chemical times, respectively. Then, a comparison is made between this solution and a numerical solution of the PaSR model equations using a Monte-Carlo technique. This comparison evidences the number of particles required for an accurate numerical computation, which is a function the aforementioned ratios.

MATHEMATICAL FORMULATION

It is supposed that the adiabatic PaSR is continuously fed by a single inlet, which injects into the reactor a certain amount of homogeneously premixed fuel and oxidizer. A single product results, represented by the mass fraction progress variable $c = (T - T_0)/(T_{ad} - T_0)$, $0 \leq c \leq 1$, and T, T_0 and T_{ad} are the temperature, the entrance temperature and the adiabatic combustion temperature, respectively. Thus, at the entrance of the reactor $c = 0$. Also, simultaneous withdrawal from the reactor of an equal amount of the resulting mixture occurs. Then, the pdf transport equation for the PaSR model is derived formally from the full transport pdf equation by assuming that, within the reactor volume, statistically homogeneous conditions prevail and accounting for inlet and outlet flows. Considering that the chemical process is described by a single-step Arrhenius reaction, and that molecular mixing (micro-mixing) obeys the Interaction by Exchange with the Mean (IEM or LMSE) model and, for the simplicity, assuming the density to be constant, the governing equations for a PaSR may be written as the first order partial differential equation [9, 11–13]:

$$\frac{\partial P(\theta;t)}{\partial t} = \underbrace{\frac{1}{\tau_m}\frac{\partial}{\partial \theta}\left[\theta - \bar{c}(t)\right] P(\theta;t)}_{\text{(I)}} + \underbrace{\frac{1}{\tau_r}\left[\delta(\theta) - P(\theta;t)\right]}_{\text{(II)}} - \underbrace{\frac{1}{\tau_c}\frac{\partial}{\partial \theta}\,\dot{\omega}(\theta)\, P(\theta;t)}_{\text{(III)}}. \quad (1)$$

Reference [13] contains a wealth of information on PaSR models: how the equations are derived, for which cases analytical solutions are known. However, the case of the present article is not yet included. In Eq. 1, t is the time, θ is the sample space variable that corresponds to the random variable—reactive scalar c, τ_r is the residence time within the PaSR ($\tau_r = \rho V/\dot{m}$, where ρ is the density, V is the volume of the reactor and $\dot{m}$ is the mass flow rate), τ_m and τ_c are the characteristic times of the micro-mixing and chemical processes, respectively. The terms (I), (II), and (III) describe, respectively, micro-mixing, inlet and outlet flows (forcing), and chemistry. Equation 1 is non-homogeneous because of the forcing term (II). It has to be stressed that Eq. 1 is, in fact, an integro-differential equation, because the mean concentration value $\bar{c}$ (which is also the average of θ within the reactor) is determined by:

$$\bar{c}(t) = \int_{-\infty}^{+\infty} \theta P(\theta;t)\, d\theta. \quad (2)$$

The δ-function in the forcing term (II) corresponds to the inlet flow with $\theta = 0$ and pdf $P(\theta;t)$ corresponds to outlet flow. The δ-function leads to, as it will be shown later, finite probability flux at the boundary $\theta = 0$ of the phase space, that is, $\lim_{\theta \to +0} \{[\theta - \bar{c}(t)]/\tau_m - \dot{\omega}(\theta)/\tau_c\}\, P(\theta;t) \neq 0$.

The chemical reaction source term, $\dot{\omega}(\theta)$ is described by an Arrhenius law and, for an adiabatic reactor, where the temperature may

be directly related to the progress variable c [$T = T_0 + (T_{ad} - T_0)c$], one has, for a first order kinetic (see e.g. [14]):

$$\dot{\omega}(\theta) = (1 - \theta) \exp\left(\beta \frac{\theta}{\theta + 1/\alpha}\right), \quad (3)$$

where $\alpha = (T_{ad} - T_0)/T_0$ is the reduced heat of reaction and $\beta = E/RT_0$ is the reduced activation energy, $T = T_0(1 + \alpha c)$. In fact, the exponential term in Eq. 3 represents the product exp (E/RT_0) exp $(-E/RT)$, thus the coefficient exp (E/RT_0) is also included in the definition of τ_c. This chemical source term is not the trivial one, and this choice is dictated by the aim to simulate the main features of detailed, high activation energy, chemical kinetic.

Introducing two dimensionless ratios x and y, which are the ratios between the residence time and the mixing and chemical times, respectively, Eq. 1 is rewritten as

$$\frac{\partial P(\theta;t)}{\partial \tau} = x \frac{\partial}{\partial \theta}[\theta - \bar{c}(t)] P(\theta;t) + [\delta(\theta) - P(\theta;t)] - y \frac{\partial}{\partial \theta} \dot{\omega}(\theta) P(\theta;t), \quad (4)$$

where $\tau = t/\tau_r$, $x = \tau_r/\tau_m$ and $y = \tau_r/\tau_c$. The parameter x is characteristic of the relationship between macro- and micro-mixing processes. The well-known Perfectly Stirred Reactor (PSR) model corresponds to the case when $x \to \infty$, that is, when $\tau_m \ll \tau_r$, while y remains finite. In this limit case of absence of scalar fluctuations, micro-mixing occurs instantaneously (infinitely fast), that is, the the pdf is a Dirac δ-function

$$P(\theta;\tau) = \delta[\theta - \bar{c}(\tau)]. \quad (5)$$

In this case, Eq. 4 degenerates, and it is sufficient to solve only the equation for the mean concentration, which is closed in this limit:

$$\frac{d\bar{c}}{d\tau} = -\bar{c} + y\dot{\omega}(\bar{c}). \quad (6)$$

Equation 6 is obtained if Eq. 4 is multiplied by θ and integrated over all values of θ, and accounting for Eq. 5.

The other limit case, which corresponds to $x = 0$, is characterized by the absence of micro-mixing, in which the steady-state solution of the PaSR model is reduced to a plug flow solution convoluted with the particle age distribution function (sometimes also called residence time distribution), that is, with the exponential function $\tau_r^{-1} \exp(-t/\tau_r)$ [6]. Thus, the shape of the pdf is expected to be qualitatively very different for $x \gg 1$ and $x \ll 1$. The parameter y is the Damköler number based on the residence time, that is, a macro-mixing time. The usual definition of the Damköler number is Da $= \tau_m/\tau_c$ that is, Da $= y/x$.

SOLUTION OF THE PDF TRANSPORT EQUATION

Equations 1 and 4 contain, along with smooth functions, a generalized Dirac δ-function located at $\theta = 0$. One can seek for solutions of 1 and 4, following the technique developed in [2], in the form:

$$P(\theta;\tau) = [H(\theta) - H(\theta - 1)] g(\theta;\tau), \quad \tau > 0, \quad (7)$$

where H is the Heaviside step-wise function and g is a continuous function in the range $0 \le \theta \le 1$, at any finite τ. Thus, Eq. 4 becomes:

$$[H(\theta) - H(\theta - 1)] \frac{\partial g(\theta;\tau)}{\partial \tau} = x[\delta(\theta) - \delta(\theta - 1)][\theta - \bar{c}(\tau)] g(\theta;\tau) + x[H(\theta) - H(\theta - 1)] \frac{\partial}{\partial \theta}[\theta - \bar{c}(\tau)] g(\theta;\tau) + \delta(\theta) - [H(\theta) - H(\theta - 1)] g(\theta;\tau) - y[\delta(\theta) - \delta(\theta - 1)] \dot{\omega}(\theta) g(\theta;\tau) - y[H(\theta) - H(\theta - 1)] \frac{\partial}{\partial \theta} \dot{\omega}(\theta) g(\theta;\tau). \quad (8)$$

First, Eq. 8 is multiplied by the function of concentration $\psi(\theta)$, which is assumed to be an arbitrary "good" function. This function has the derivatives that will be needed hereafter. Then, this product is integrated over θ from $-\infty$ to ∞ and, using the well-known rules of operations with generalized functions, one may obtain:

$$\int_0^1 \psi(\theta)\left\{\frac{\partial g(\theta;\tau)}{\partial \tau} - x\,\frac{\partial}{\partial \theta}\left[\theta - \bar{c}(\tau)\right] g(\theta;\tau) + g(\theta;\tau) + y\,\frac{\partial}{\partial \theta}\,\dot{\omega}(\theta) g(\theta;\tau)\right\} d\theta + x\psi(0) g(0;\tau)\bar{c}(\tau)$$

$$+ x\psi(1) g(1;\tau)[1 - \bar{c}(\tau)] - \psi(0) + y\psi(0)\dot{\omega}(0) g(0;\tau) - y\psi(1)\dot{\omega}(1) g(1;\tau) = 0. \quad (9)$$

The function $\psi(\theta)$ is arbitrary, hence, the integral and all the coefficients multiplying $\psi(0)$ and $\psi(1)$ in the equation above must each be identically equal to zero. As a consequence, one obtains the equation for the smooth function g:

$$\frac{\partial g(\theta;\tau)}{\partial \tau} = \frac{\partial}{\partial \theta}\,/(\theta;\tau) g(\theta;\tau) - g(\theta;\tau), \quad (10)$$

where

$$r(\theta,\tau) = x\,[\theta - \bar{c}(\tau)] - y\dot{\omega}(\theta), \quad (11)$$

and boundary conditions

$$g(0;\tau)[x\bar{c}(\tau) + y\dot{\omega}(0)] = 1 \Leftrightarrow g(0;\tau) r(0,\tau) = -1, \quad (12)$$

$$g(1;\tau)\,\{x[1 - \bar{c}(\tau)] - y\dot{\omega}(1)\} = 0 \Leftrightarrow g(1;\tau) r(1,\tau) = 0. \quad (13)$$

Taking into account that $\dot{\omega}(0) = 1$ and $\dot{\omega}(1) = 0$, [(Eq. 3)], the boundary conditions, that is Eqs. 12 and 13, are written as:

$$g(0;\tau) = 1/[x\bar{c}(\tau) + y], \quad \tau > 0, \quad (14)$$

$$g(1;\tau) = 0, \quad \tau > 0. \quad (15)$$

Note that function g$(\theta;\tau)$ is non-zero at $\theta = 0$ due the presence of a δ-function in Eq. 4. Also, the value of x should be different from zero ($x \neq 0$), otherwise the value of $g(1;\tau)$ is indeterminate and may not be prescribed.

To summarize, the pdf time evolution, that is, the Cauchy problem, is described by a first order partial differential equation (Eq. 10), together with boundary conditions Eqs. 14 and 15 [for $x = 0$ only Eq. 14 is used] and by the initial pdf at $\tau = 0$:

$$g(\theta;\tau) = g_0(\theta), \quad 0 < \theta < 1, \quad \tau = 0. \quad (16)$$

The solution of this problem can be found by the method of characteristics (see e.g., [15]). The equations for the characteristic curves in the (g, θ, τ) space are written as:

$$\frac{d\theta}{d\tau} = -r(\theta,\tau), \quad (17)$$

$$\frac{d\ln g}{d\tau} = r'(\theta,\tau) - 1 \quad (18)$$

where the prime denotes the derivative with respect to θ.

Note that, for g to be a realizable pdf, it has to be non-negative and to satisfy to the normalization condition. The first of these conditions is ensured by Eq. 18, provided that g is initially non-negative.

As sketched in Fig. 1, the projections of the characteristic curves on the plane (τ,θ) evolve in an open rectangular region, $0 < \theta < 1$, $\tau > 0$, beginning from the points situated at the boundary of this region, i.e., given by initial conditions at $\tau = 0$:

$$\theta = \theta_0, \quad 0 < \theta_0 < 1, \quad \tau = 0, \quad (19)$$

$$g = g_0(\theta_0), \quad \tau = 0, \quad (20)$$

where g_0 is the initial pdf (Eq. 16) and by boundary conditions Eqs. 14 and 15, when $\tau > 0$.

The solution of Eqs. 17 and 18, subjected to conditions 19, 20, 14, and 15, gives the parametric representation of the pdf time evolution for given θ_0, that is $\theta = \theta(\theta_0;\tau)$, $g = g(\theta_0;\tau)$. Eliminating this parameter from this solution, yields the pdf in explicit form, $g(\theta;\tau)$.

The qualitative behavior of the projections of the characteristic curves $\theta(\tau)$ on the plane (θ,τ) is given in Fig. 1 (a). In this figure $\theta_*(\tau)$ is the root of the function $r(\theta,\tau)$, that is

$$r(\theta_*,\tau) = x\,[\theta_* - \bar{c}(\tau)] - y\dot{\omega}(\theta_*) = 0. \quad (21)$$

Because $r(0) < 0$ and $r(1) > 0$, such a point always exists (here it is supposed that $x \neq 0$). Note that Eq. 21 is similar to the PSR steady-state equation [14] and, when chemistry is described by an Arrhenius law, it could have, in the general case, multiple solutions (up to three roots). However, it is important to underline

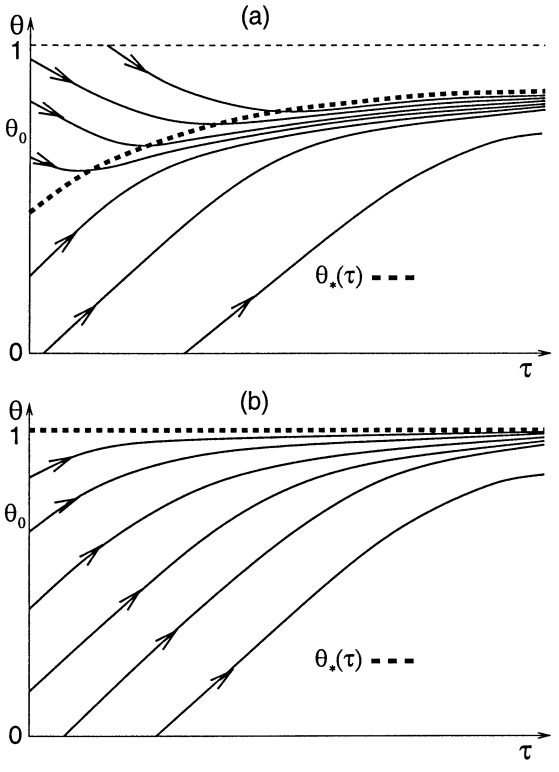

Fig. 1. Schematic representation of the projections of the characteristic lines on the (θ, τ) plane: (a) $x \neq 0$, $\theta_*(\tau \to \infty) \to \theta_* = \text{const.} \neq 1$, (b) $x = 0$, $\theta_*(\tau) = 1$.

that, as opposed to the PSR case, the solution of Eq. 21 is implicitly dependent of the pdf overall shape, because it includes the mean concentration value $\bar{c}$ (Eq. 2). Thus, finding θ_* requires to solve first the pdf equation (Eq. 10).

It is interesting to note, however, that there are two (above mentioned) limiting cases, when θ_* can be obtained without this cumbersome procedure. The first one corresponds to the absence of micro-mixing, that is, $x = 0$. Eq. 21 takes the form

$$y\dot{\omega}(\theta_*) = 0, \tag{22}$$

which leads, after Eq. 3, to

$$\theta_*(\tau) = 1, \tag{23}$$

for all values of y. In this case the projections of the characteristic curves are sketched in Fig. 1 (b). In this figure it can clearly be seen that the value of $g(1;\tau)$, $\tau > 0$ has not been prescribed beforehand, as is the case when $x \neq 0$ in Fig. 1 (a).

The second case corresponds to the PSR limit, $x \to \infty$, when the pdf is a Dirac δ-function Eq. 5. In this case

$$\theta_*(\tau) = \bar{c}(\tau), \tag{24}$$

where $\bar{c}(\tau)$ is given by Eq. 6.

The transient behavior of the pdf is not the object of the present study, which is further restricted to the analysis of the limiting steady-state solutions. Thus, the time variable in all functions is omitted hereafter. Only one consequence which follows from Eqs. 17, 18, and boundary and initial conditions 19, 20, 14, and 15 will be used here, that is, that the steady-state solution is identically zero in the range:

$$g(\theta) \equiv 0; \quad \theta_* \leq \theta \leq 1. \tag{25}$$

Note that, as depicted in Fig. 1 (a), $\theta_* = \text{const}$ is the limit to which tends $\theta_*(\tau)$ as $\tau \to \infty$. Moreover, as opposed to Eq. 7, in which $g(\theta;\tau)$ is a continuous pdf at any finite τ, the limit steady-state pdf is, as will be seen later, generally discontinuous.

Thus, the steady-state pdf is the solution of the following initial value (Cauchy) problem for the ordinary differential equation:

$$(rg)' = g \qquad 0 \leq \theta \leq \theta_*, \tag{26}$$

$$g(0) = 1/(x\bar{c} + y), \tag{27}$$

together with two integral conditions:

$$\int_0^{\theta_*} g(\theta)d\theta = 1, \tag{28}$$

$$\bar{c} = \int_0^{\theta_*} \theta g(\theta)d\theta. \tag{29}$$

Equations 28 and 29 are the normalization condition and the definition of the mean concentration, respectively. It should be noted that the normalization condition is not independent, as it follows from the application of the initial value condition Eq. 27 (or Eq. 12), after integration of Eq. 26 over $0 \leq \theta < \theta_*$:

$$(rg)\Big|_0^{\theta_*} = [rg]_{\theta\to\theta_*} - r(0)g(0) = \int_0^{\theta_*} g(\theta)\, d\theta. \tag{30}$$

The limit of the product $[rg]_{\theta\to\theta^*}$ is equal to zero, as will be seen below, and thus, following Eq. 12, the normalization condition is always fulfilled, even if $\bar{c}$ is an arbitrary parameter, which does not coincides with the mean concentration.

Differential Eq. 26 can be easily transformed in an integral equation, by integrating it once:

$$g(\theta)r(\theta) = g(0)r(0)\,\exp\left[\int_0^{\theta} r^{-1}(s)\, ds\right]; \qquad 0 \le \theta \le \theta_*. \tag{31}$$

Using the boundary condition (Eq. 12), one obtains finally the integral equation:

$$g(\theta) = -\frac{1}{r(\theta)}\exp\left[\int_0^{\theta}\frac{1}{r(s)}\, ds\right], \quad 0 \le \theta < \theta_*. \tag{32}$$

The above formulated problem, described by Eqs. 26–29 and 32, is the main analytical result of the present work. The immediate and important consequence of Eq. 32 is that the function $r(\theta)$ has to be negative to ensure the realizability of g.

As a first step to proceed with the numerical calculations, Eq. 32 is used to study the asymptotic behavior of g in the left vicinity of θ_*. This study is required since $r(\theta_*) = 0$, which leads to an indeterminacies of Eq. 32. Thus, one may write

$$r(\theta) = r'(\theta_*)(\theta - \theta_*), \quad 0 < \epsilon = (\theta_* - \theta) \ll 1, \tag{33}$$

For simplicity here the case of a single root is analyzed. Similar considerations can be made when θ_* is the repeated root of order 2. Substituting Eq. 33 in Eq. 32 yields:

$$g(\theta) \to A\epsilon^k, \quad \epsilon \to 0, \tag{34}$$

$$k = 1/r'(\theta_*) - 1, \tag{35}$$

where A is a constant that should be determined by matching the global solution of the problem, Eqs. 26–29 with the asymptotics Eqs. 34–35.

It is seen that the steady-state solution has relevance only if $k > -1$, that is, if $r'(\theta_*) > 0$. This condition is automatically satisfied if $r(\theta)$ is negative (as is also needed for $g(\theta)$ to be positive) in the domain $0 \le \theta < \theta_*$. In the case $0 < r'(\theta_*) < 1$, $k > 0$ and the pdf g is equal to zero at $\theta = \theta_*$, that is, $g(\theta_*) = 0$.

It can be seen from Eqs. 34–35 that, for the case $r'(\theta_*) > 1$, $-1 < k < 0$ and, as a consequence, the pdf has an integrable singularity at $\theta = \theta_*$. Note, however, that the asymptotic behavior of the product rg is $rg \to Ar'(\theta_*)\epsilon^{1+k}$, that is, $rg \to 0$ as $\epsilon \to 0$, which was used above to prove that the normalization condition is always verified.

Computations are performed for typical values of parameters $\alpha = 0.8$ and $\beta = 15$, which correspond to a high activation energy, moderate heat release chemical reaction. The parameters x and y are varied in the ranges $0 \le x \le 10$ and $0.001 \le y \le 10$. As a reference point, in Fig. 2 (a) the steady-state PSR solution

$$\hat{c} = y\dot{\omega}(\hat{c}). \tag{36}$$

is given versus the y parameter. It is seen that the solution of Eq. 36, that is, $\hat{c}$ as a function of y, yields, for the chosen values of α and β, the so-called S-shaped curve, which is three-valued in the domain $y_1 \le y \le y_2, y_1 = 0.0107, y_2 = 0.03674$. The curve $\hat{c}(y)$ has the vertical tangents in the points $y = y_1$ and $y = y_2$, that is, $dy/d\hat{c} = 0$. The equations for the determination of y_1 and y_2 are [14]

$$\frac{T_{1,2}}{T_0} = \frac{(2+\alpha)\beta \pm \sqrt{\alpha\beta[\alpha\beta - 4(1+\alpha)]}}{2(\alpha+\beta)}, \tag{37}$$

$$c_{1,2} = \left(\frac{T_{1,2}}{T_0} - 1\right)\frac{1}{\alpha} = \frac{\alpha(\beta-2) \pm \sqrt{\alpha\beta[\alpha\beta - 4(1+\alpha)]}}{2\alpha(\alpha+\beta)}, \tag{38}$$

$$y_{1,2} = \frac{c_{1,2}}{\dot{\omega}(c_{1,2})}. \tag{39}$$

The former point (y_1) corresponds to extinction, the latter one to ignition. The upper and lower branches of the S-shaped curve correspond to the intensive and the weak stable combustion regimes in the PSR, respectively. The middle (intermediate) branch corresponds to the unstable regimes.

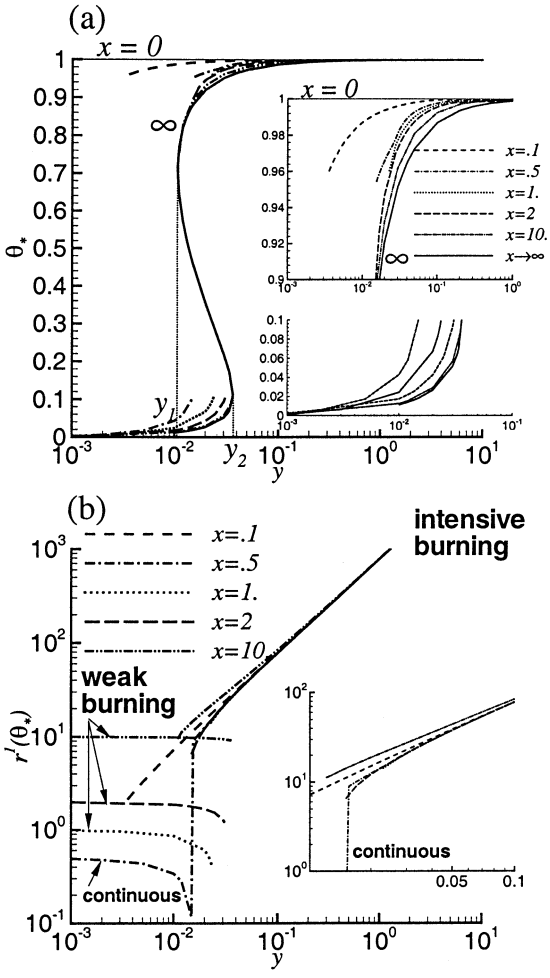

Fig. 2. Values of θ_* and $r'(\theta_*)$ as functions of y for different values of x, $\alpha = 0.8$, $\beta = 15$, y_1 and y_2 are the extinction and ignition points for the PSR, $y_1 = 0.0107$, $y_2 = 0.03674$.

Because the PaSR solution approaches the PSR limit at $x \to \infty$, one could expect that, if x is greater than some critical value x_{cr}, the PaSR pdf solutions exhibit a similar qualitatively behavior. There is a domain $0 < y < y_1'$ where there is only one stable steady-state pdf with low-valued amplitudes of θ corresponding to a PaSR that does not ignite (weak combustion regimes), a domain $y_1' < y < y_2'$ where there are three steady-state pdfs, two of which are stable and correspond to weak and intense combustion regimes—the latter with high-valued amplitudes of θ—and, finally, a domain $y > y_2'$ where there is, once again, only one steady-state pdf with high-valued amplitudes of θ. Beyond a critical value, $x < x_{cr}$, in the whole range of y, there is only one steady-state pdf, corresponding to a continuous mode of PaSR operation. As for the case of the PSR, this continuous mode can also be obtained by the reduction of β [14].

The chosen numerical solution procedure of the problem Eqs 26–29 involves a shooting method, where some guess value of $\bar{c}$ is prescribed. Equation 26 is integrated numerically from $\theta = 0$ to $\theta_1 = \theta_* - \epsilon$, and Eqs. 34–35 are used in the interval $\theta_1 < \theta < \theta_*$ in order to satisfy the normalization condition of the pdf and to compute the contribution to the different statistical moments of the values of θ lying in the range $\theta_1 < \theta < \theta_*$. The computed value of $\bar{c}$ is compared to the prescribed one: if a given tolerance is achieved, the computation is halted, otherwise the computed value of $\bar{c}$ is used in the place of the previously prescribed one, and the integration procedure is restarted. As the value of k increases, smaller values of ϵ are required for the convergence of this numerical procedure. Since, in the general case, Eq. 21 has multiple solutions, both the initial value of $\bar{c}$ and the boundaries of the domain where the root θ_* is sought (by a combination of bisection and Newton-Raphson methods [16]) must be carefully chosen. A continuation procedure, in which y is either progressively increased/decreased for a given value of x is also used. In this procedure, the prescribed initial value of $\bar{c}$ is the one obtained for the previous value of y. Also, the computations are found to require the use of quadruple precision on an HP-PA 7200, 32-bit arithmetic, processor.

The computational results presented in Fig. 2 (a) confirm, in general terms, the above-described picture of PaSR operation. It is seen that θ_* increases with y and decreases with x. If x is greater than a critical value x_{cr} (in particular, when $x > 1$), the curve $\theta_*(y)$ is similar to the above-mentioned S-shaped curve for the PSR, and there exists a range of values of the parameter y for which the two stable roots of Eq. 21 are obtained. For the chosen values of α and β, this critical value is found to lie in the range $0.5 < x_{cr} < 1$.

The upper branch with larger values of θ_* (for $x > x_{cr}$) corresponds to intensive combustion regimes, while the lower one, with smaller ones are related to weak burning regimes within the PaSR. These regimes are limited by the

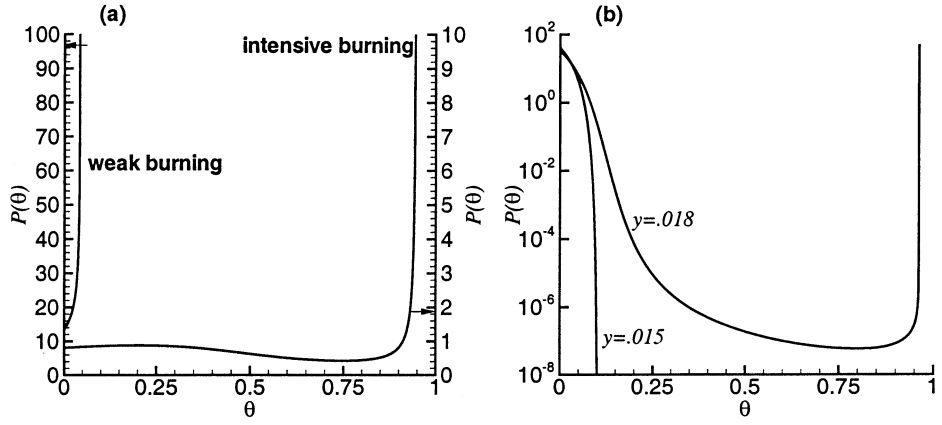

Fig. 3. Steady-state pdfs of the progress variable for (a) $x = 2$ and $y = 0.02$ ($x > x_{cr}, y_1' < y < y_2'$), (b) $x = 0.5$ and $y = 0.0115$ and 0.018 ($x < x_{cr}$).

ignition and extinction events as for the PSR. Critical values y_1' and y_2' of the parameter y at which these events take place are analogous to the above-defined parameters y_1 and y_2 within the PSR, but the exact values of y_1' and y_2' depend of x. As the value of x is decreased, the range of y where two stable solutions are possible decreases and, eventually, beyond a critical value, $x \leq x_{cr}$, vanishes, that is, ignition and extinction are suppressed, and the θ_* (y) transforms to a monotonous, single-valued, curve.

As stated above, it is expected that, when $x > x_{cr}$, unstable regimes of combustion exist within the PaSR, in the domain $y_1' < y < y_2'$, which would be analogous to those found in the PSR. These regimes would correspond to the middle branch (intermediate values of θ_*). It is quite probable that steady-state pdf solutions corresponding to these unstable regimes do not exist. In particular, calculations attempted of the steady-state pdf, using the above-described numerical procedure, were not successful in these unstable regimes. The problem of existence of unstable steady-state PaSR pdfs deserves further investigation.

The evolution of $r'(\theta_*)$ with y is given in Fig. 2 (b). Typical values of $r'(\theta_*)$ lie in the range (0.1, 1000). It is seen that the corresponding range of k is such that direct finite difference solution of Eq. 26 will meet with difficulties, for the larger values of $r'\theta_*$), without a proper treatment of the singular point θ_*. The asymptotic analysis presented above allows to overcome this problem. For the case when θ_* corresponds to the intense combustion regimes, $r'(\theta_*)$ increases with y and is practically independent of x. On the contrary, in the case of weak combustion regimes, $r'(\theta_*)$ is almost constant with y and increases with x.

Figure 3 (a) shows the resulting pdfs corresponding to values of x and y where two steady-state solutions are possible. The overall shapes of the pdfs are rather distinct. In the case of weak burning, P is a monotonously increasing function of θ, and most values of θ are "forbidden" [$P(\theta) \equiv 0$] within the PaSR since θ_* is small. In the case of intensive burning, the pdf first increases, then decreases with θ, presenting a rather "flat" distribution for intermediate values of θ, before tending to ∞ as θ_* is approached. In Fig. 3 (b) are plotted the steady-state pdfs corresponding to $x = 0.5 < x_{cr}$, $y = 0.015$ and 0.018, for which the average of the progress variable $\bar{c}$ is 0.019 and 0.024, respectively. Although the shape of the pdfs are rather similar for small values of θ, there is an important difference for larger values of θ. In the former case, $\theta_* = 0.102$ and $g(\theta_*) = 0$, while in the latter case, $\theta_* = 0.962$ and $g(\theta_*) \to \infty$. Also, when $y = 0.018$, the value of P for the intermediate range of θ is extremely small. This distinctive change of shape of the pdf and the abrupt increase of both θ_* and $r'(\theta_*)$ illustrate the sensitivity of the steady-state solution to small changes of the controlling parameters x and y.

In Fig. 4 are presented the computed pdf for some particular values of the ratios between the residence time and the micro-mixing and chemical times, x and y. The smaller values of y, 0.01

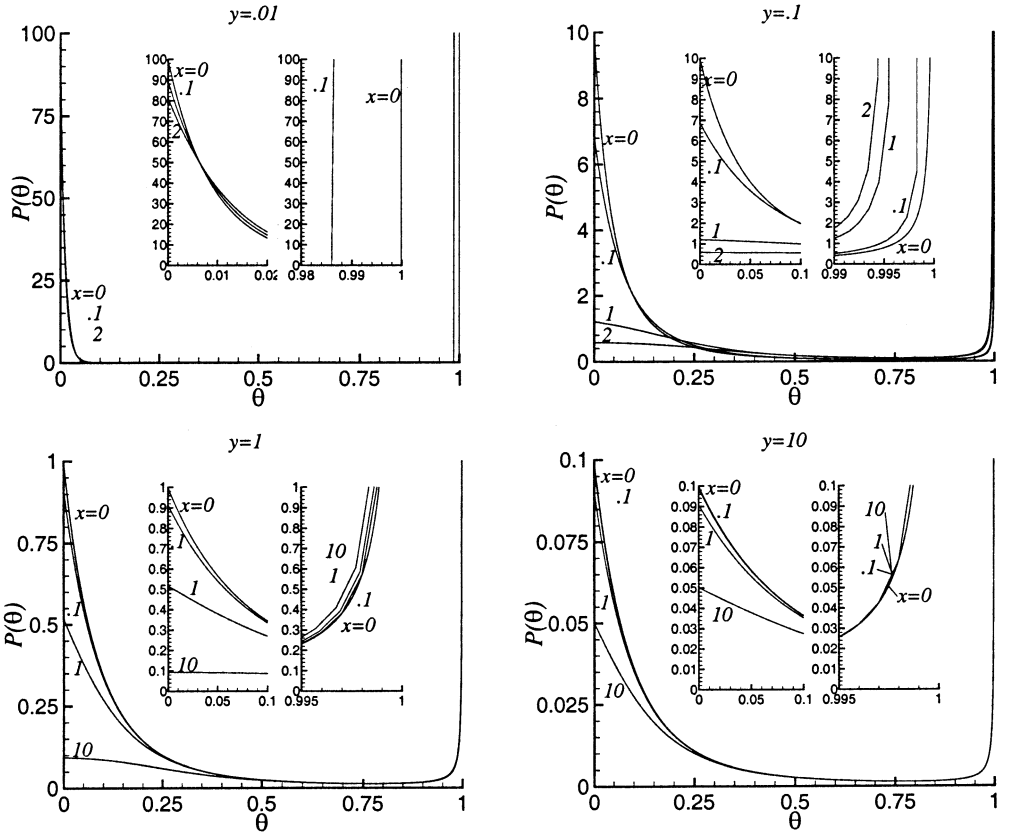

Fig. 4. Steady-state pdfs of the progress variable for various values of x and y.

and 0.1, correspond to cases where the only possible steady-state solution is the weak combustion regime, while, for the larger values of y, 1 and 10, only intense steady-state combustion regimes should occur within the PaSR. The pdf for the particular case of no micro-mixing ($x = 0$ and given y) is also given in Fig. 4. In this case, as shown above, $\theta_* = 1$ (Eq. 23), and it follows from Eq. 32 that

$$g(\theta) = \frac{1}{y\dot{\omega}(\theta)} \exp\left[-\int_0^\theta \frac{1}{y\dot{\omega}(s)}\, ds\right], \quad 0 \le \theta < 1. \tag{40}$$

The asymptotic behavior of g in the vicinity of $\theta = 1$, as can be easily found from Eqs. 3 and 40, is described by

$$g(\theta) \to \frac{1}{a_0 y}(1-\theta)^{-1+1/a_0 y}, \qquad a_0 = \exp\left(\frac{\beta}{1+1/\alpha}\right). \tag{41}$$

Note that the value of the pdf at the boundary $\theta = 1$ strongly depends on the value of the product $a_0 y$: $a_0 y < 1$ leads to $g(1) = 0$, while $a_0 y > 1$ implies $g(1) \to \infty$.

As indicated above, the solution of Eq. 40 is a plug flow reactor solution convoluted with the particle age distribution function $f(t)$, that is, with the exponential function $f(t) = \tau_r^{-1} \exp(-t/\tau_r)$. Indeed, for one realization of total duration t_1, the change of concentration $\theta(t_1)$ within the PaSR may be found from the plug flow reactor equation

$$\frac{d\theta}{dt} = \frac{1}{\tau_c}\dot{\omega}(\theta), \quad 0 \le t < t_1. \tag{42}$$

Thus, the conditional pdf is

$$P(\theta|t = t_1) = \delta(\theta - \theta_1), \quad \theta_1 = \theta(t_1). \tag{43}$$

The unconditional pdf is determined by the integration of Eq. 43 multiplied by $f(t_1)$ over all values of t_1

$$P(\theta) = \int_0^\infty P(\theta|t = t_1)\, f(t_1)\, dt_1$$

$$= \int_0^\infty \delta(\theta - \theta_1)\tau_r^{-1} \exp(-t_1/\tau_r)\, dt_1. \quad (44)$$

Equation 44 is equivalent to Eq. 40. To verify this, t_1 should be written (using Eq. 42) as a function of θ_1:

$$t_1(\theta_1) = \tau_c \int_0^{\theta_1} \frac{ds}{\dot{\omega}(s)}, \quad dt_1 = \frac{\tau_c}{\dot{\omega}(\theta_1)}\, d\theta_1, \quad (45)$$

and then the basic δ-function property should be used:

$$\int_0^\infty \delta(\theta - \theta_1) F(\theta_1)\, d\theta_1 = F(\theta), \quad (46)$$

where F is an arbitrary continuous function. It has to be noted that the same technique could be used here to obtain the steady-state solution for the case $x \neq 0$, Eq. 32. It is sufficient to replace $\omega(\theta_1)$ by $-r(\theta_1)$, however, this is not a direct way to prove that $g \equiv 0$ in the range $\theta_* < \theta < 1$.

Figure 4 shows that, when the micro-mixing and chemical times are smaller than the residence time, that is, when both x and y are larger than 1, the pdfs are dominated by the peak that occurs at the vicinity of θ_* and the PaSR solution is qualitatively similar to the PSR model. Note the change in the scale of the vertical axis. This result is in full correspondence with the value of the pdf at the boundary $\theta = 0$, which is given by Eq. 27. It is seen from this equation that the values of the pdf in the vicinity of $\theta = 0$ decrease when either x or y increase. When either x or y are decreased, the probability of finding unreacted gases within the PaSR increases and the pdfs become increasingly bi-modal. This leads to a decrease of the average value of the progress variable within the reactor, as it can be verified in Fig. 5(a), where the evolution of the average $\bar{c}$ with y is given for various values of x. The corresponding evolution of the standard deviation (SD) $\sigma = \sqrt{\overline{(c - \bar{c})^2}}$ is given in Fig. 5 (b). Also shown in this figure is the value $\hat{c}$ corresponding to the solution of the PSR model ($x \to \infty$).

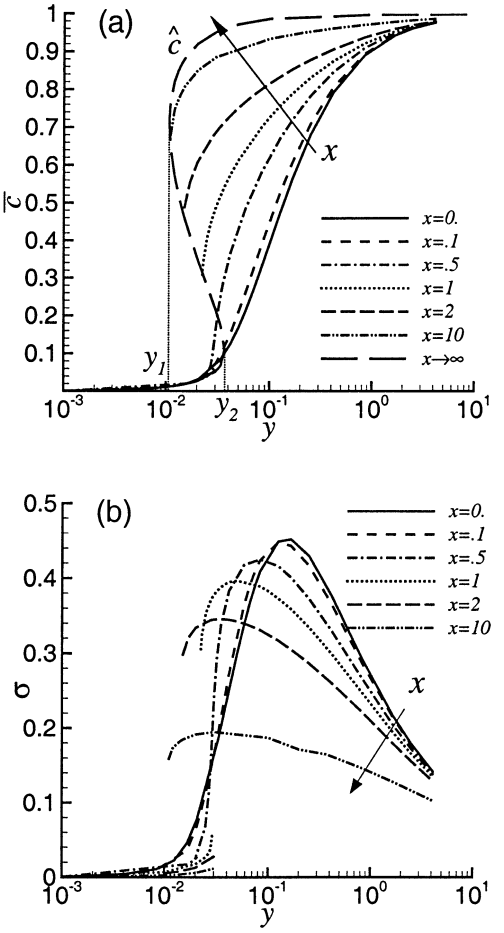

Fig. 5. Average (a) and SD (b) of the progress variable as a function of y for different values of x; y_1 and y_2 are the extinction and ignition points for the PSR, $y_1 = 0.0107, y_2 = 0.03674$. Parameter changes are indicated by arrows.

The most notable influence on the mean concentration curve of the micro-mixing effects is its qualitative change when x decreases from ∞. As it can be verified in Fig. 5 (a), for values of x which are smaller than some above-mentioned critical value ($0.5 < x_{cr} < 1$, for the chosen values of α and β, see discussion above), the S-shaped curve for the mean concentration $\bar{c}$ transforms to a monotonic continuous function of y. The blowout, which is typical of the S-shaped curves, is absent for these values of x. Figure 5 (a) also shows that

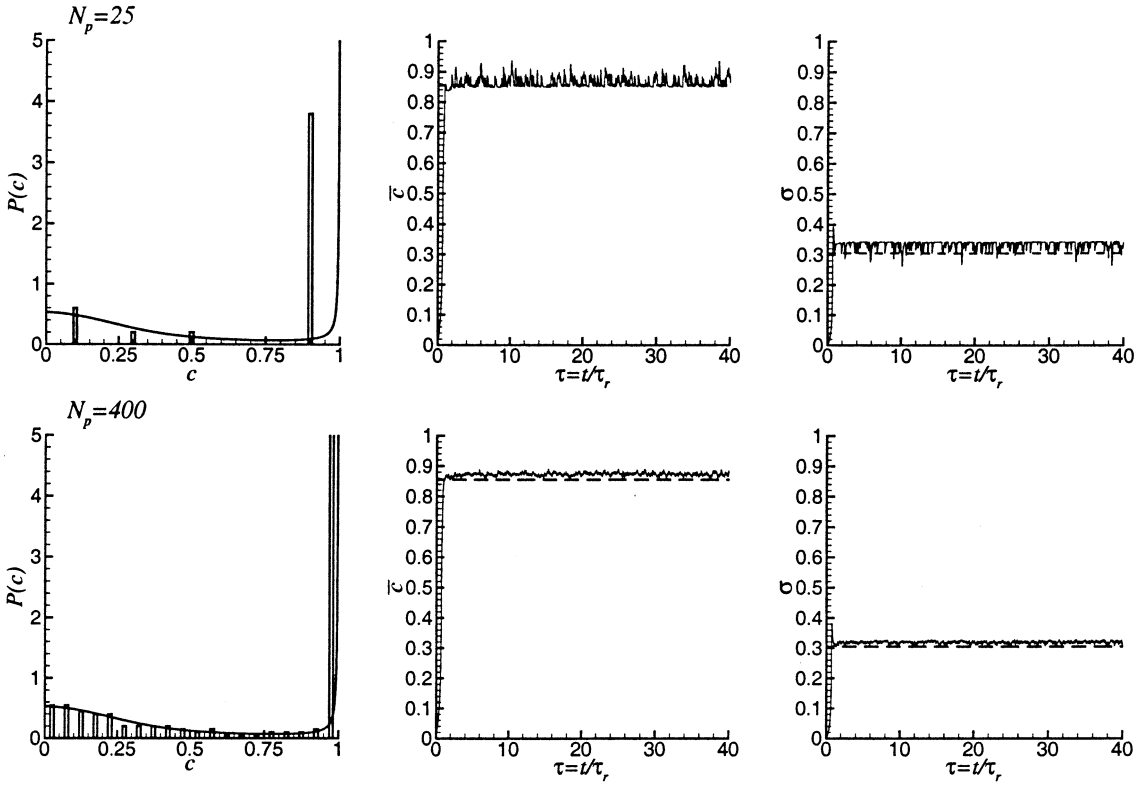

Fig. 6. Comparison between theoretical (lines)—and simulated (histograms) steady-state pdfs of c and history of the ensemble average and standard deviation of c for $x = 2$ and $y = 0.167$, for different number of stochastic particles N_p. This case corresponds to the intensive regime of combustion, that is $x > x_{cr}$ and $y > y_2'$. The dotted line corresponds to the theoretical steady-state values of $\bar{c}$ and σ, 0.855 and 0.305, respectively.

when x increases $\bar{c} \to \hat{c}$, that is, the PaSR approaches the PSR limit.

Because decreasing the characteristic micromixing time leads to a homogenization of the composition within the reactor, the standard deviation σ decreases when x increases from zero, for a given value of y, as seen in Fig. 5 (b). However, the standard deviation exhibits a nonmonotonous behavior with y. When the characteristic chemical time τ_c is increased, and thus y is decreased, first σ increases from zero at $y \to \infty$, reaches a maximum, then decreases: σ is equal to zero when $y = 0$. If the value of x is less than the above indicated critical value, which is the case for $0 \leq x \leq 0.5$ in Fig. 5 (b), σ decreases continuously to zero with y. At values of x which are greater than the critical value, the maximum of σ is located at the vicinity of y_1'. It is quite probable in this case that the maximum value nearly corresponds to PaSR blowout. It would be interesting to further analyse this question in more detail using more sophisticated calculation methods.

MONTE-CARLO SOLUTION OF THE PASR MODEL EQUATION

The Monte-Carlo simulation of a PaSR is described in [6, 9], and is shortly recalled here. The reactor volume contains N_p particles, each characterized by a given value of the concentration $c^{(n)}, n = 1, \ldots, N_p$. At each time step, Δt, N_e particles are randomly selected and withdrawn from the reactor [16]. These N_e particles are immediately replaced by an equal amount of particles consisting of fresh unburned gases ($c = 0$). Thus, the residence time is calculated as $\tau_r = N_p\ \Delta t/N_e$. Between selection and withdraw, the

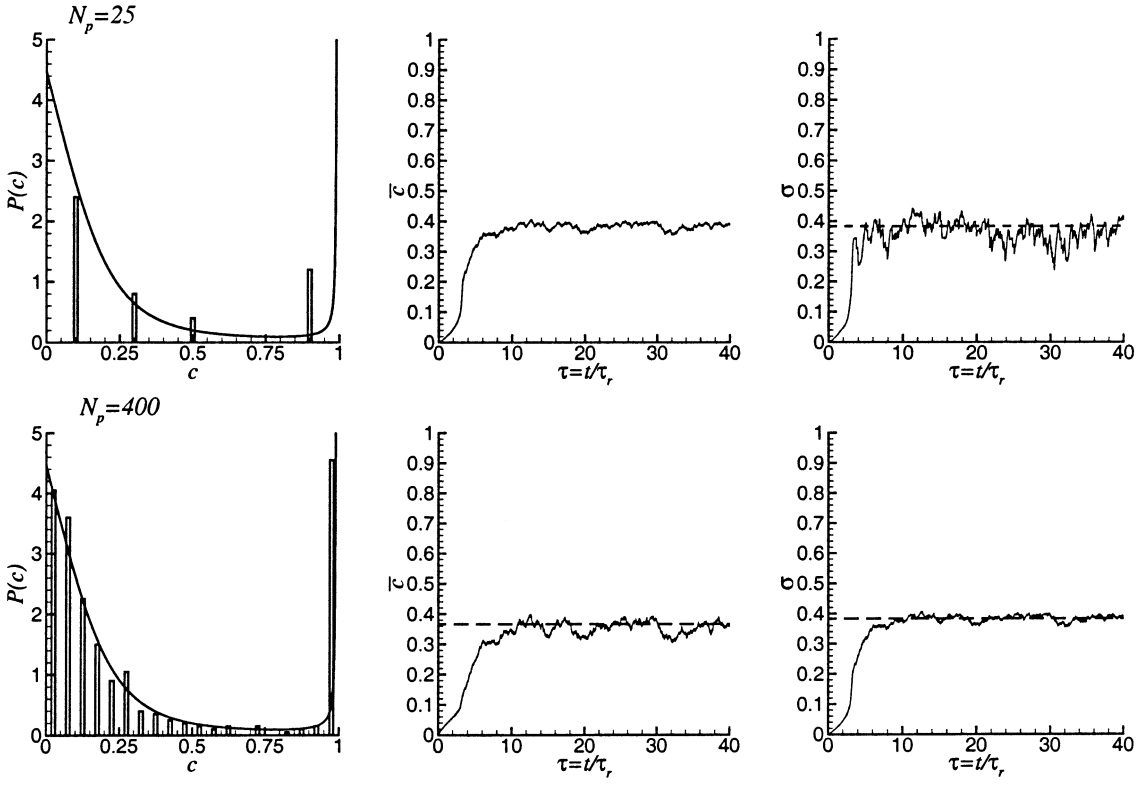

Fig. 7. Comparison between theoretical (lines)—and simulated (histograms) steady-state pdfs of c and history of the ensemble average and standard deviation of c for $x = 0.5$ and $y = 0.042$, for different number of stochastic particles N_p. This case corresponds to the continuous regime of combustion, that is $x < x_{cr}$. The dotted line corresponds to the theoretical steady-state values of $\bar{c}$ and σ, 0.366 and 0.383, respectively.

concentration values of the particles evolve due to micro-mixing and chemical reaction, that is,

$$\frac{dc^{(n)}}{d\tau} = -x\,(c^{(n)} - \bar{c}) + y\dot{\omega}\,(c^{(n)});$$

$$n = 1, \ldots, N_p. \tag{47}$$

At the beginning of the computation all the stochastic particles contain only fresh unburned gases [$c(\tau = 0) = 0$]. For the sake of generality, the chemical kinetic term is uncoupled from the mixing term and integrated using VODE [17], which is tailored for the solution of stiff ordinary differential equations.

In Fig. 6 are plotted the pdfs of concentration c given by the solution of Eq. 26 and the histograms simulated by the Monte-Carlo method for $x = 2, y = 0.167$, and two different numbers of stochastic particles $N_p = 25$ and 400, and for one value of the number of withdrawn particles $N_e = 1$. In this case of fast micro-mixing and chemistry, $x > x_{cr}$ and $y > y_2'$, that is, intensive burning regime ($\bar{c} = 0.855$) occurs within the PaSR. Also plotted in this figure are the respective histories of the averaged value of $\bar{c}$ and of its standard deviation, σ. Figure 7 shows the corresponding pdfs, histograms and histories obtained for the case of slow micro-mixing and chemistry, $x = 0.5$ and $y = 0.042$ ($x < x_{cr}$, i.e., the continuous mode of combustion takes place within the PaSR). Results presented in Figs. 6 and 7 are obtained for values of x and y for which only one solution exists for the pdf equation.

For the initial conditions chosen here, performing computations for other values of x and y, such that either intensive or weak burning regimes are possible, that is $x > x_{cr}$ and $y_1' < y < y_2'$ (led to the weak combustion regime only. However, it is possible to envisage initial condi-

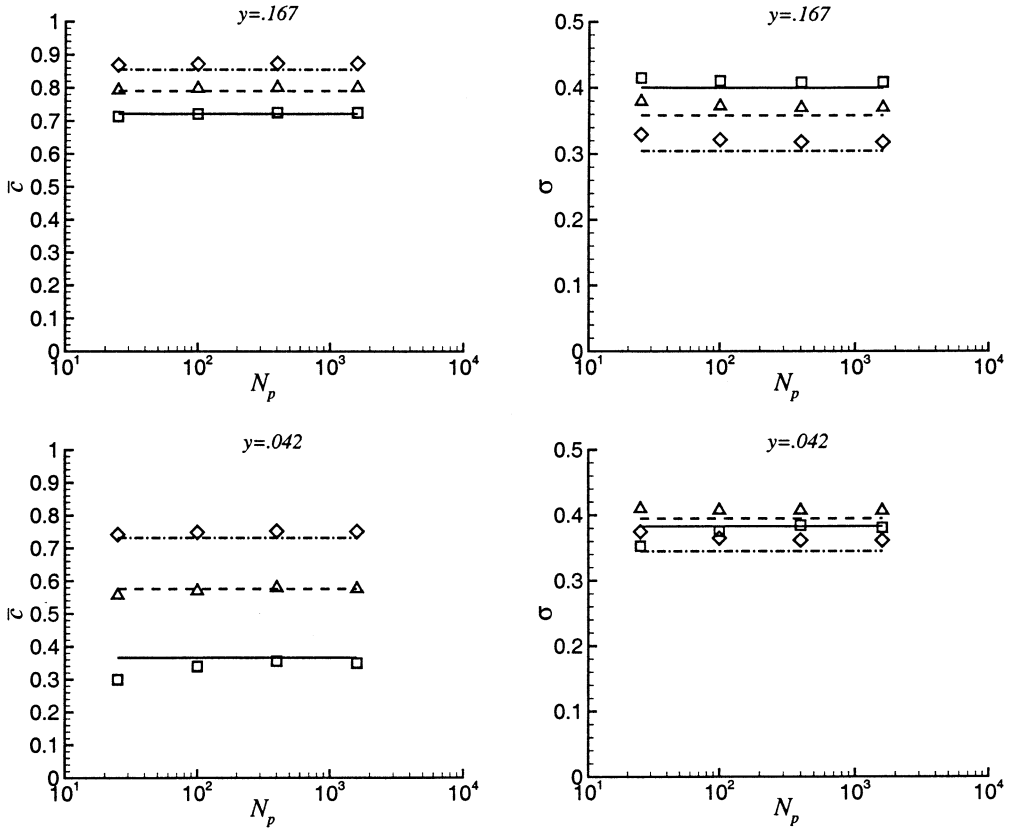

Fig. 8. Comparison between theoretical (horizontal lines) and simulated (symbols) values of the ensemble average and standard deviation of c as a function of the number of stochastic particles for $x = 0.5$: —, □; 1: – –, △; and 2: –·–, ◇.

tions corresponding to stochastic particles that are already burning at $\tau = 0$ which could lead to the intensive burning regime for such values of x and y.

These figures show that the overall histogram shape is correctly recovered when both mixing and chemistry are fast or slow, even when $N_p = 25$. The time evolution of $\bar{c}$ and σ exhibit a small dispersion around their mean values for $x = 2$, $y = 0.167$ for both values of N_p chosen. On the other hand, for the case when $x = 0.5, y = 0.042$, $\bar{c}$ and σ are found to substantially fluctuate around their mean values even when $N_p = 400$. One can explain these augmented stochastic fluctuations, when compared to the case $x = 2$ and $y = 0.167$ above (shown in Fig. 6), by the pronounced bi-modal shape of the pdf when micro-mixing is slow with respect to the residence time. Physically, it is clear that more particles are needed to represent the pdf with two peaks.

As seen in Figs. 6 and 7, in general a good agreement is obtained between the values of $\bar{c}$ and σ resulting from the numerical simulation and those obtained by integration of Eq. 26. This can also be verified in Fig. 8, where the values of $\bar{c}$ and σ computed by the Monte-Carlo simulation (symbols) for different values of the number of particles, N_p are compared to those obtained by direct integration of the pdf transport equation (horizontal lines), for two values of y, 0.167 and 0.042, and three values of x, 0.5, 1 and 2. Indeed, this figure shows that, when $N_p \geq 100$, an excellent agreement is always obtained. However, when $N_p = 25$, discrepancies are found to occur. Moreover, for a given number of stochastic particles, the match between the Monte-Carlo simulation and direct solution of the pdf is better when both chemistry and mixing are fast when compared to the residence time of the mixture.

As it could be expected, the fluctuations around the mean values of $\bar{c}$ and σ decrease as

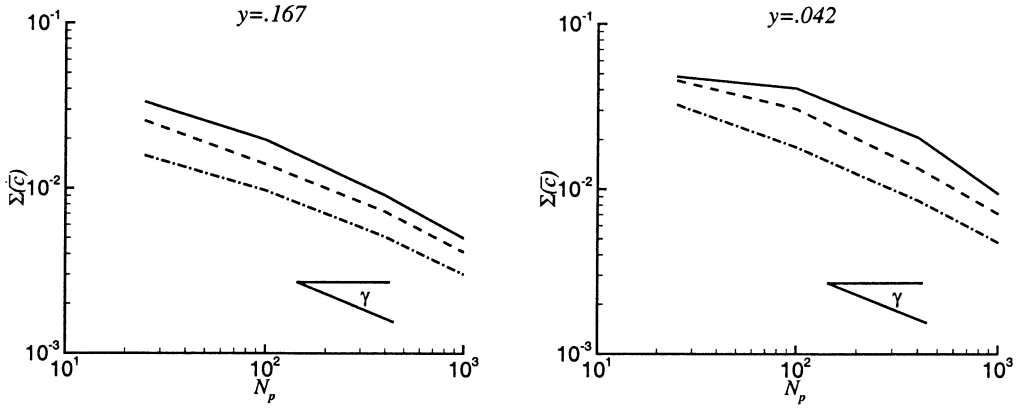

Fig. 9. Standard deviation of the fluctuations around $\bar{c}$ as a function of the number of stochastic particles for $x = 0.5$: —; 1: – –; and 2: –·–. The angle γ corresponds to a $-1/2$ slope.

N_p is increased in the Monte-Carlo simulation. This can be verified in Fig. 9, where the behavior of the standard deviation of the fluctuations around $\bar{c}$ (noted Σ, to avoid confusion with the standard deviation σ of the stochastic variable c) is given for the same values of N_p, x, and y as in Fig. 8. Analogous trends, not given here, are obtained for the fluctuations around σ. This figure also shows that, for a given number of stochastic particles N_p used in the Monte-Carlo simulation, decreasing x or y leads to an increase of $\Sigma(\bar{c})$.

CONCLUSIONS

The transport equation for the pdf of a single reacting scalar within a PaSR has been solved directly and modeled via a Monte-Carlo simulation. The shape of the steady-state pdfs and thus, the statistical moments of the scalar were found to be dependent on the ratios between the overall residence time and the micro-mixing time and the characteristic chemical times. In particular, significant departures from the PSR solutions were found as these ratios are decreased and approach one. The Monte-Carlo solution of the model equation has been shown to yield a good agreement with the direct pdf solution when the ratio between the number of stochastic particles and the number of withdrawn particles is larger than 100. However, a large scattering of the different statistical moments computed is observed when the aforementioned ratios decrease. The exact relevance of these results for the computation of pollutant formation will be assessed in future works.

The authors would like to thank the anonimous reviewers for their valuable and stimulating comments.

REFERENCES

1. Peters, N., *Prog. Energy Combust. Sci*. 10:319–339 (1984).
2. Kuznetsov, V. R., and Sabel'nikov, V. A. *Turbulence and Combustion*. Hemisphere Publishing Corp., New York, 1990.
3. Bray, K. N. C., and Peters, N., in *Turbulent Reacting Flows*, (P.A. Libby and F.A. Williams, Eds.), Academic Press Inc., 1994, pp. 63–113.
4. Borghi, R., *Prog. Energy Combust. Sci*. 14:245–292 (1988).
5. Klimenko, A. Y., and Bilger, R. W., *Prog. Energy Combust. Sci*. 25:595–687 (1999).
6. Correa, S. M., *Combust. Flame* 93:41–60 (1993).
7. Correa, S. M., and Braaten, M. E., *Combust. Flame* 94:469–486 (1993).
8. Correa, S. M., Hu, I. Z., and Tolpadi, A. K., *J. Energy Ress. Technol*. 118:201–208 (1996).
9. Pope, S. B., *Prog. Energy Combust. Sci*. 11:119–192 (1985).
10. Chen, J. Y., *Combust. Sci. Technol*. 122:63–94 (1997).
11. Pope, S. B., *Combust. Flame* 27:299–312 (1976).
12. Bonniot, C., and Borghi, R., *Acta Astronautica* 6:309–327 (1979).
13. Kraft, M., *Stochastic Modeling of Turbulent Reacting Flow Chemical Engineering*, Fortschritt-Berichte VDI, Reihe 6 Energietechnik, Nr. 131, VDI Verlag, Dusseldorf, 1998.
14. Zel'dovich, Ya.B., Barenblatt, G. I., Librovich, V. B., and Makhviladze, G. M. *The Mathematical Theory of Combustion and Explosions*. Consultants Bureau, New York, 1985.

15. Sneddon, I. N. *Elements of Partial Differential Equations*. McGraw-Hill, New York, 1957.
16. Press, W. H., Teukolsky, S. A., Vettering, W. T., and Flannery, B. P. *Numerical Recipes in FORTRAN: The Art of Scientific Computing* (2nd ed.). Cambridge University Press, 1994.
17. Byrne, G. D., and Dean, A. M., *Comput. & Chem*. 17:297–302 (1993).

Received 18 April 2001; revised 12 December 2001; accepted 26 December 2001